PNAS
www.pnas.org

Supplementary Information for

PI16 controls neuropathic pain: a potential role of meningeal fibroblasts

Pooja Singhmar[1], Ronnie The Phong Trinh[1], Jiacheng Ma[1], XiaoJiao Huo[1], Bo Peng[2], Cobi J Heijnen[1], Annemieke Kavelaars*[1]

1 Laboratories of Neuroimmunology, Department of Symptom Research, The University of Texas MD Anderson Cancer Center, Houston, Texas 77030, USA.
2 Department of Bioinformatics & Computational Biology, The University of Texas MD Anderson Cancer Center, Houston, Texas 77030, USA.

Correspondence: Dr. Annemieke Kavelaars, 1515 Holcombe Blvd, Unit 384, Houston, TX 77030. Phone: (713) 794-5297. Email: akavelaars@mdanderson.org

This PDF file includes:

Supplementary text
Figures S1 to S12
SI References

www.pnas.org/cgi/doi/10.1073/pnas.1913444117

SI Material and Methods

Animals. Male and female B6:129S mice homozygous for global Pi16 deletion (MMRRC stock number 032520-UCD) and their wild type control littermates at an age of 8-12 weeks were used in the study. All procedures were performed following the ARRIVE guidelines, and are in accordance with National Institutes of Health Guidelines for the Care and Use of Laboratory Animals and the Ethical Issues of the International Association for the Study of Pain (1). Studies were approved by the Institutional Animal Care and Use Committee of the University of Texas MD Anderson Cancer Center. All pain measures and immunofluorescence analyses were performed by investigators blinded to treatment.

Spared nerve injury model. SNI surgery was performed as described previously (2, 3). Briefly, mice were anesthetized under isoflurane and the three peripheral branches of the left sciatic nerve (sural, common peroneal and tibial) were exposed. The common peroneal and tibial nerves are tightly ligated and then transected distal to the ligation. The sural nerve was kept intact. For sham surgery, nerves were exposed but not ligated or transected. Von Frey measurements were performed starting from 4 days after SNI surgery. All biochemical and immunofluorescence assays were done at an early (d4-d8) and/or late (d22-d45) time point post SNI.

Measurement of mechanical allodynia. Mechanical allodynia was measured as the hind paw withdrawal response to von Frey hair stimulation and the 50% paw withdrawal threshold was calculated using the up-and-down method (4). Decrease in paw-withdrawal threshold is indicative of mechanical allodynia. In brief, animals were placed on a wire-grid base, through which the von Frey hairs (Stoelting, Wood Dale, IL, USA) with bending force range from 0.02 to 1.4 g were applied. Clear paw withdrawal, shaking, or licking was considered as nociceptive-like responses.

Cell culture and reagents. Mouse perineurial fibroblasts (M1710-57, ScienCell Research Laboratories) were cultured in complete fibroblast medium (ScienCell Research Laboratories catalog number 2301) per the manufacturer's instructions. For differentiation of fibroblasts to myofibroblasts 5ng/ml of TGF-β1 (7666-MB, R&D Systems) was used. HUVEC cell (PromoCell C-12203) were cultured in Endothelial Cell Growth medium (PromoCell C-22210) supplemented with Supplmix (C-39215). L cells (ATCC® CRL-2648) were cultured in high glucose Dulbecco's modified Eagle medium (GE Healthcare, Piscataway, NJ, USA) plus 10% fetal bovine serum (Gibco, Carlsbad, CA, USA). L cells were transiently transfected with Pi16-tGFP (Origne MG219996) and pm-Turq-ER (Addgene 36204) with Lipofectamine 2000 (Invitrogen, Grand Island, NY, USA) according to the manufacturer's instructions. To prepare conditioned medium, L cells were seeded in 6-well plates and incubated overnight, followed by transfection with 1.5 µg of Pi16-tGFP plasmid. The medium was replaced with serum free DMEM and transfected cells were incubated for 48 hours. Cell supernatant was collected from culture and centrifuged to pellet debris and dead cells and filtered through a 0.2µm

filter. Supernatant from untransfected or Pi16-tGFP transfected cells was diluted with fresh medium (1 part of fresh medium to 2 parts of supernatant) to get control conditioned medium and Pi16 conditioned medium) respectively.

Real-time quantitative PCR. The first-strand cDNA was synthesized using one-to-two µg of RNA using high capacity cDNA reverse transcription kit (Applied Biosystems) and qPCR was performed on an Applied Biosystems ViiA using Taqman primers (Integrated DNA Technologies, Coraville, IA, USA). Relative quantitative measurement of target gene levels corrected for GAPDH or β-actin was performed using the ΔΔCt method. Primers used were as follows: Human PI16 (IDT, Hs.PT.58.39664750) and Mouse Pi16 (IDT, Mm.PT.58.8467939 and Mm.PT.58.22010817).

RNA extraction, library preparation for sequencing, and RNA-seq Data analyses. Transcriptional changes in the lumbar DRGs were investigated using whole-genome RNA sequencing by the RNA Sequencing Core Lab at MD Anderson Cancer Center. RNA-seq was performed on triplicate samples and the RIN number for all samples was >7. Mice were perfused intracardially with chilled PBS and lumbar DRGs (L3–L5) were collected without desheathing the meninges. DRGs were collected 5 hours after the PGE_2 or vehicle treatment from WT and GRK2+/- mice and 9 days post SNI or Sham surgery from WT and Pi16-/- mice. DRGs were homogenized in TRIzol reagent (Invitrogen, Carlsbad, CA, USA) and total RNA was extracted with an RNeasy MinElute Cleanup Kit (Qiagen, Hilden, Germany). For RNA-seq from GRK2+/- mice, DRGs were pooled from two mice to get one sample.

The sample libraries were generated using the Stranded mRNA-Seq kit (Kapa Biosystems, Wilmington, MA) following the manufacturer's guidelines. A 75-nt paired-end run format was performed using a HiSeq 4000 Sequencer as previously described (5). Six samples were sequenced in a single lane. RNA sequencing data analysis was performed using a comprehensive in-house RNASeq pipeline, which used STAR to align paired-end reads to the mouse reference genome (mm10 version) and featureCounts to obtain expression counts of genes. The quality of raw and aligned reads was assessed using FastQC, RSeQC, and qualimap. In both GRK2+/- and Pi16-/- analyses, we used principal component analysis and unsupervised hierarchical clustering to analyze and samples and R Bioconductor packages EdgeR and DESeq2 to compare expressions of genes between groups of interest. We excluded genes with on average less than 10 reads per samples and selected genes with adjusted p-value < 0.05 as differentially expressed. For SNI dataset, further analysis was performed with Ingenuity Pathway Analysis (IPA; Qiagen Inc., https://www.qiagenbioinformatics.com/products/ingenuity-pathway-analysis/) to identify biological processes and canonical pathways that were potentially affected by PI16 deficiency. A data set of differentially expressed genes (adjusted p<0.05) containing gene identifiers, their corresponding expression values (log_2Ratio), and P-values was uploaded on IPA for core analysis.

Immunofluorescence and microscopy. DRG (lumbar L3-L5), spinal cord, and sciatic nerve were collected from mice perfused with PBS followed by 4% paraformaldehyde in

PBS. Spinal cord meninges were gently peeled with forceps from the vertebrae in a single layer. Tissues were cryo-protected in 20% sucrose and embedded and frozen in 1:1 mix of optimal cutting temperature compound (OCT; Bayer Corporation) and 20% sucrose, and sliced into 14 µm sections. Sections were permeabilized with 0.3% Triton-x-100 and blocked with normal serum (5%), saponin (0.1%), and BSA (2%) and stained with primary antibodies followed by Alexa-594, Alexa-488, or Alexa-647 conjugated secondary donkey or goat antibodies (Invitrogen, Grand Island, NY). Nuclei was stained with DAPI and for negative control, primary antibody was omitted. Sections were visualized using a Leica SPE DMI 4000B confocal microscope or EVOS fluorescence microscope. The mean intensity of fluorescence and the percent area positive were calculated using Leica or NIH ImageJ software. For TEM analysis of mitochondrial morphology, nerves were fixed in 2% glutaraldehyde plus 2% PFA in PBS and processed as previously described (6). For immunostaining, n values represent staining of a processed tissue section derived from individual mouse. For all staining, additional technical replicates were also included where different sections of the same tissue were stained and observed/imaged for consistency. For comparison between samples, sections were stained together in a single experiment. For negative control sections, primary antibody was omitted.

Western blotting. Tissue and cell lysates were prepared using Bioruptor (Diagenode) in RIPA buffer (10 mM Tris-HCl, pH 6.8, 100 mM NaCl, 1 mM EDTA, 10% glycerol, 1% Triton X-100, 0.1% SDS, 0.5% sodium deoxycholate, 2 mM Na3VO4, 50 mM NaF) supplemented with protease inhibitor cocktail and phosphatase inhibitors . Protein content was assessed using Bradford (Bio-Rad Laboratories, Hercules, CA, USA) or BCA assay (Pierce, Rockford, IL, USA). Equivalent amounts of protein or equal volume from each sample were run on SDS-polyacrylamide gels and transferred to polyvinylidene difluoride membranes (GE Healthcare, Piscataway, NJ, USA). Following blocking in 5% milk or bovine serum albumin the blots were incubated with primary antibodies and analyzed by HRP-conjugated secondary antibodies (Jackson Laboratories). The following primary antibodies were used in the study: PI16 (1:750, R&D Systems AF4929), α-SMA (1:1500, Abcam ab5694), β-Actin (1:50,000, Sigma A3854), α-Tubulin (1:2000, Cell Signaling 2144S), pMLC2 (Cell Signaling 3674S, 3675S), Chemerin (R&D Systems AF2325). For detection of signal, enhanced chemiluminescent agent (GE Healthcare, Piscataway, NJ, USA) or Clarity Western ECL Substrate (Bio-Rad, Hercules, CA, USA) was used followed by imaging on LAS4000 chemiluminescence system. Band density was determined using LAS Image Quant software (GE Healthcare, Piscataway, NJ, USA).

Sodium fluorescein permeability assay. Sodium fluorescein (Sigma Aldrich, St. Louis, MO) (40 mg/kg) was injected through the tail vein on day5 post SNI surgery and allowed to circulate for 1 hour. Mice were perfused with ice-cold PBS with heparin intracardially and nerves were collected and processed as described above in immunofluorescence section. Cross-sections of the nerve were quantified by EVOS fluorescence microscope and the mean intensity of fluorescence and the percent area positive were calculated using NIH ImageJ software.

Transwell assay. Transwell inserts (Corning 6.5mm diameter insert, 5um pore size, PET membrane, 24 well plate) were coated with collagen I (30ug/ml overnight, Gibco A10483-01) and fibronectin (7.5ug/ml for 1 hour, Corning 354008). HUVEC cells (2.0 x 104, PromoCell C-12203) were seeded in endothelial medium (PromoCell C-22210) in the inserts and grown till a confluent monolayer of cells was formed (3 days). In parallel, L cells were transfected with PI16-tGFP construct and PI16 conditioned medium was prepared. In addition, THP-1 monocytes were cultured in RPMI medium and treated with phorbol 12-myristate 13-acetate (PMA) (300 nM, 48 h) to differentiate them into monocytes. On the day of assay, HUVEC cells were activated with 500 units/ml of TNFα (210-TA-005) either in control or PI16 conditioned medium following by addition of 1 x 105 THP-1 monocytes to the top chamber. Human CXCL12 (SDF-1α, 300-28A, 50ng/ml) either in control or PI16 conditioned medium was added to the bottom chamber. Cells were allowed to migrate for 5 hours. Inserts were washed with PBS followed by fixation with 4% PFA and staining with 0.2% crystal violet. Cells on the top of the insert were removed using a cotton swab and only cells which migrated across the membrane were counted under a microscope.

SI Figures

a

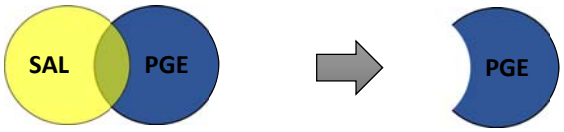

ID	gene	WT-SAL	WT-PGE	KO-SAL	KO-PGE	PGE (WT->KO) regulated	SAL (WT->KO) regulated	WT (SAL->PGE) regulated	KO (SAL->PGE) regulated
10906	ligp1	8.66	11.21	9.26	5.81	down	no	up	down
2948	Gm12250	1.38	2.18	1.62	1.20	down	no	up	no
14859	Gbp2	16.33	19.84	16.72	13.32	down	no	no	down
2950	Irgm2	8.26	10.21	7.94	6.98	down	no	no	no
9677	Pi16	22.61	15.94	23.40	21.97	up	no	down	no

b

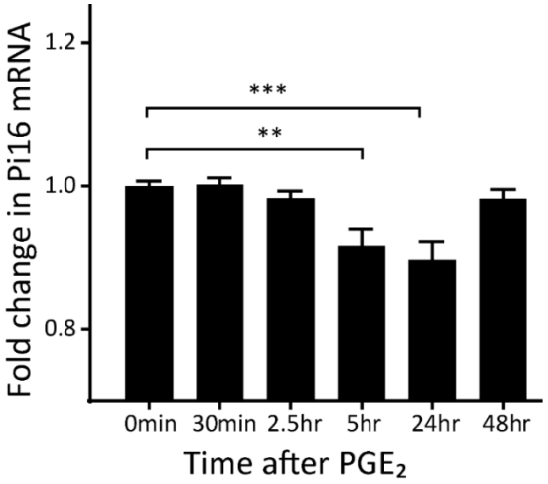

Fig. S1. (a) Normalized log-counts-per-million reads for novel differentially expressed genes (DEG) between WT and GRK2+/- (KO) mice associated with pain sensitivity. DEG were identified for the SAL group (between WT-SAL and KO-SAL) and PGE2 group (between WT-PGE2 and KO-PGE2) and the overlapping genes between the two groups were eliminated (i.e. genes that differed due to genotype). **(b)** Validation of PGE2-induced changes in PI16 mRNA by RT PCR analysis of PI16 in independent samples of lumbar DRGs of WT male mice at various time points after PGE2 treatment (100 ng/paw). GAPDH was used for normalization. n = 3 male mice per time point; One-way ANOVA followed by post hoc (Tukey) test: **P < 0.005, ***P < 0.0005.

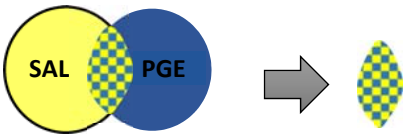

ID	gene	WT-PGE	KO-PGE	WT-SAL	KO-SAL	SAL (WT->KO) regulated	SAL (WT->KO) q_value
450	Tnni1	12.8927	4.68409	25.3463	5.53242	down	0.007541
6744	Tnnc1	23.2529	6.82758	52.729	9.62632	down	0.007541
7399	Myh7	3.59527	0.937171	6.78397	0.836385	down	0.007541
8325	Mb	60.1451	41.3157	116.967	50.5631	down	0.007541
11727	Adrbk1 (GRK2)	69.8604	42.893	66.8315	38.5189	down	0.007541
15435	Myoz2	5.92071	2.4654	9.87762	4.5512	down	0.007541
17704	Myl2	41.355	9.54716	79.603	16.624	down	0.007541
21238	Tnnt1	16.0347	4.00184	31.1835	6.06305	down	0.007541
24130	Sln	7.71582	1.69838	18.1172	2.15711	down	0.007541
24501	Myl3	17.2083	4.33783	28.6223	5.24341	down	0.007541
1782	Prtn3	18.1083	27.3485	26.9032	19.0768	down	0.013198
1783	Elane	18.6586	27.7646	27.8844	18.3039	down	0.007541
1785	Cfd	80.721	125.635	145.331	94.0642	down	0.007541
3035	Myh1	2.30788	5.42612	5.90265	3.5096	down	0.007541
3106	Eno3	25.929	41.5637	71.2126	49.1519	down	0.007541
3251	Slfn4	2.22643	3.47022	3.78227	2.30737	down	0.007541
3303	Mpo	10.8255	16.3733	15.8396	10.5542	down	0.007541
3681	Pgam2	11.9112	18.978	32.4448	18.0839	down	0.007541
4418	Slc4a1	22.3193	29.3149	27.9448	20.391	down	0.022787
6491	Cmya5	1.80324	2.47959	4.10177	2.98727	down	0.018415
7193	Myoz1	6.85066	13.6969	27.3086	18.8787	down	0.031464
8750	Adipoq	13.1821	19.9494	22.9245	15.4039	down	0.007541
11739	Actn3	10.1665	18.9589	40.4975	27.5767	down	0.026934
13413	Lcn2	107.925	154.006	157.345	116.103	down	0.013198
13568	Ttn	0.451306	0.621851	0.900694	0.510824	down	0.007541
16436	Tpm2	23.2742	32.4952	63.7371	35.3539	down	0.007541
17551	Ibsp	9.26908	13.3032	17.4578	12.1261	down	0.031464
18268	Igj	7.20812	11.2176	9.26268	4.50295	down	0.007541
19860	Cidec	8.9779	13.318	13.6596	8.06286	down	0.007541
20270	Ckm	66.6505	121.217	229.849	157.882	down	0.007541
21502	Cd177	6.71992	9.94331	8.70326	5.44563	down	0.007541
23661	Hp	26.482	40.0049	38.1018	25.0785	down	0.007541
23782	Acta1	104.288	145.984	277.514	167.528	down	0.007541
24497	Ngp	230.858	323.462	307.812	228.971	down	0.040608
24511	Ltf	38.6149	55.1005	49.2932	32.4304	down	0.007541
25885	Alas2	52.6075	70.2154	80.5557	59.0525	down	0.007541
7617	Dct	0.359117	1.34026	0.744143	1.92369	up	0.007541
15784	Tyrp1	5.12758	11.0774	6.51297	11.872	up	0.007541
24855	Zbtb16	1.284	2.39998	1.03602	2.48913	up	0.007541

Fig. S2. Normalized log-counts-per-million reads for DEG that differed due to GRK2+/- genotype between WT-SAL and KO-SAL.

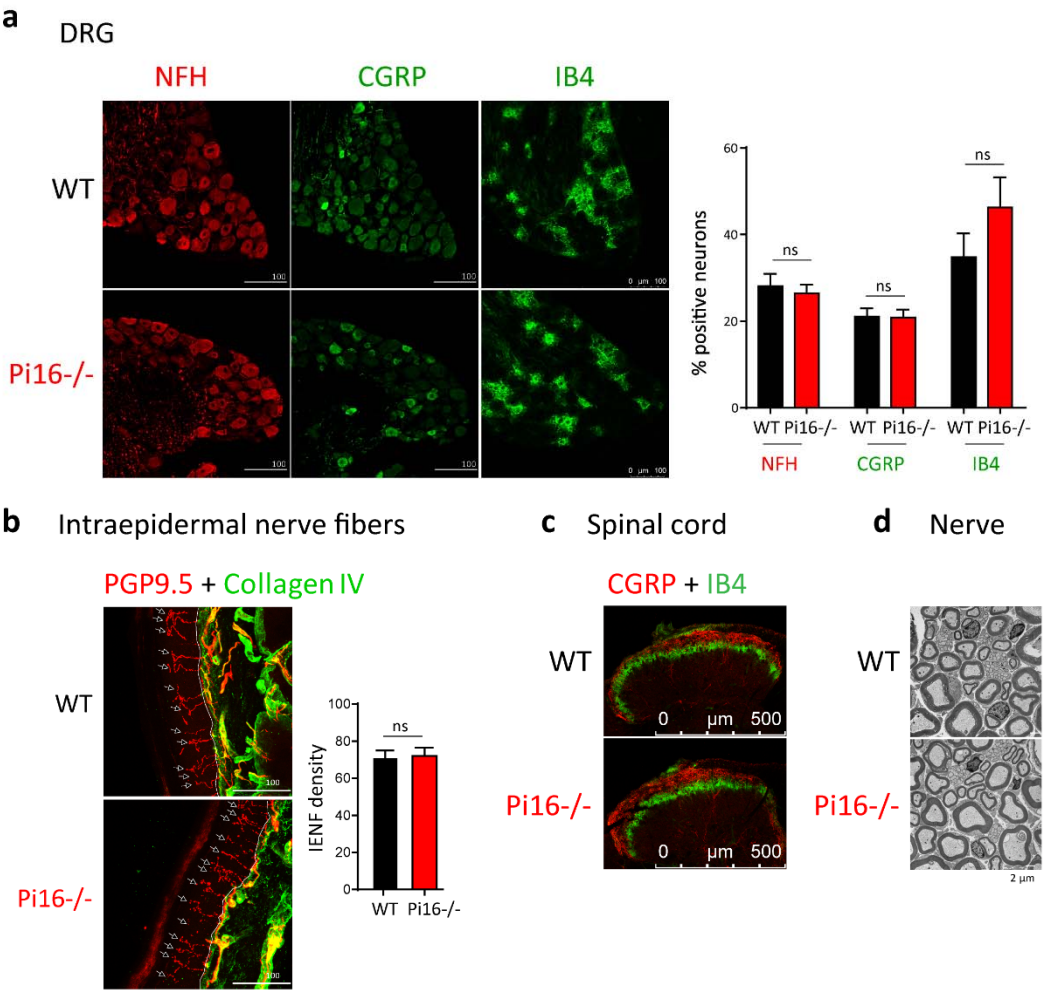

Fig. S3. Pi16-/- knockout mice have normal distribution pattern of neuronal subpoupulations. **(a)** Representative images showing lumbar DRG rom WT and Pi16-/- mice stained for NF200 A-fiber neurons (NFH), CGRP peptidergic neurons, and IB4 nonpeptidergic neurons in lumbar-DRGs Scale bar indicates 100 µm. Bar graph represents percent of neurons staining positive for each marker. No significant differences were observed between WT and Pi16-/- mice. **(b)** Immunostaining with pan-neuronal marker PGP9.5 (red) and basement collagen membrane (green) to identify IENFs in hind paw skin sections from WT and Pi16-/- mice. Representative confocal images show IENF (white arrows) crossing the basement collagen membrane. Bar graph shows IENF density expressed as number of nerve fibers crossing the basement membrane/length of the basement membrane. Scale bar indicates 100 µm. **(c)** Representative image of lumbar spinal cord of WT and Pi16-/- mice stained for CGRP peptidergic neurons and IB4 nonpeptidergic neurons. **(d)** Electron micrograph of a sectioned sciatic nerve from WT and Pi16-/- mice showing normal myelin wrapping and nerve fiber structure. Scale bar indicates 2 µm.

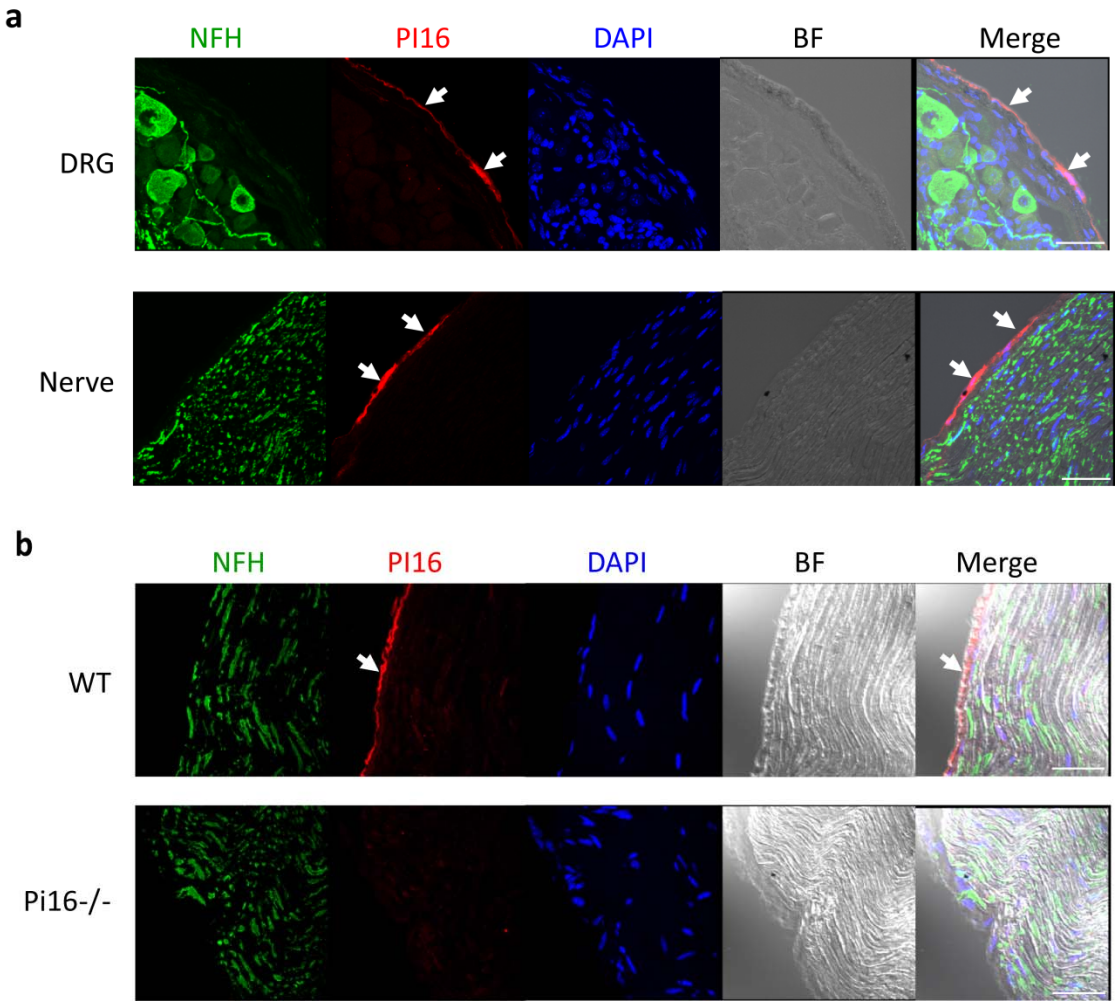

Fig. S4. PI16 is localized in the meninges of DRG and the epi/perineurium of nerve. Additional representative images stained with the neuronal marker NFH, DAPI, and PI16 of **(a)** lumbar DRG and sciatic nerve sections from WT mice, **(b)** sciatic nerve sections from WT and Pi16-/- mice. Scale bar: 50 µm (a) and 75 µm (b).

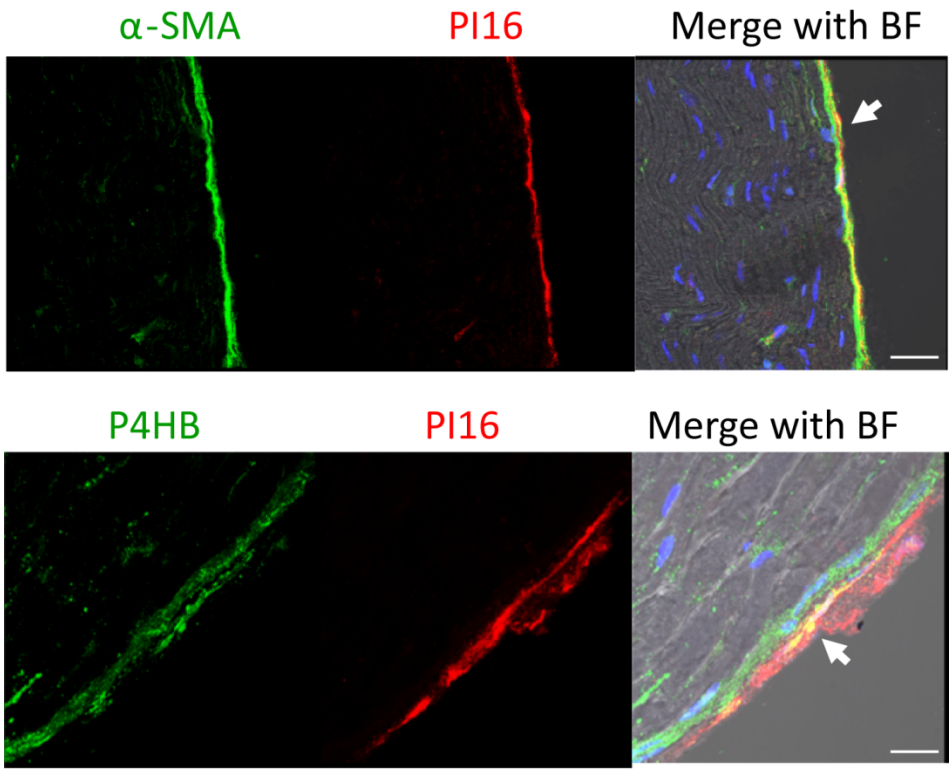

Fig. S5. Lower magnification images of sciatic nerve section showing PI16 (red) is detected in fibroblasts (green) in the epi/perineurium. Blue staining is DAPI. Scale bar: 25 µm.

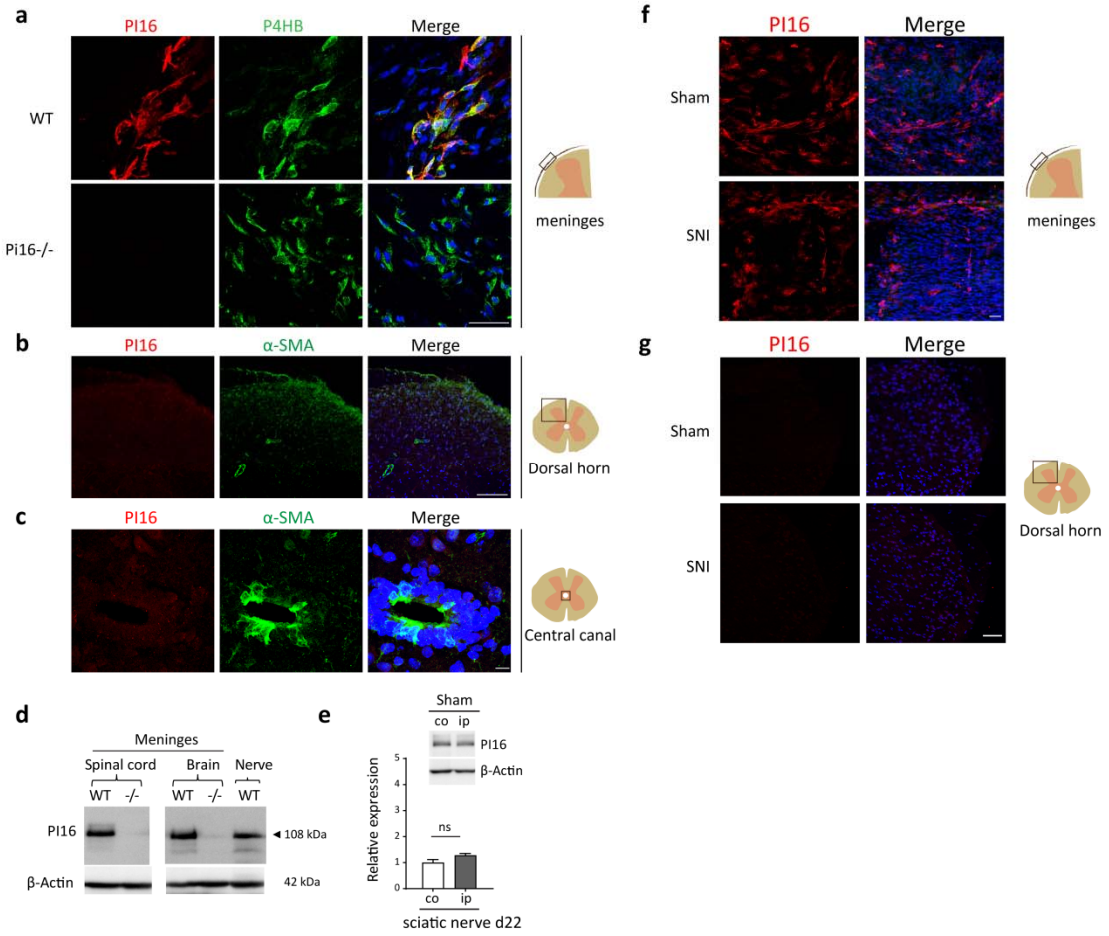

Fig. S6. PI16 is expressed in fibroblasts in the meninges of spinal cord and SNI does not induce changes in spinal cord PI16 expression. **(a)** Representative image of spinal cord meninges from naïve WT and Pi16-/- mice stained with PI16 (red) and fibroblast marker P4HB (green). **(b)** and **(c)** Representative spinal cord section from naïve WT mice showing dorsal horn area, b and central canal, c stained with PI16 (red), α-SMA (green), and DAPI (blue). Scale bar indicates 50 µm for a, 100 µm for b, and 10 µm for c. **(d)** Western blot analysis showing PI16 protein expression (detected as a 108kDa band) in spinal cord and brain meninges from naïve animals. **(e)** Western blot analysis of PI16 protein expression in ipsilateral (ip) and contralateral (co) sciatic nerve at 22 days after Sham surgery (t test, ns not significant). **(f)** Representative image showing PI16 (red) and DAPI (blue) staining in spinal cord meninges in WT mice after Sham or SNI surgery (day 5). **(g)** Representative image of spinal cord section showing dorsal horn of ipsilateral side stained with PI16 (red) and DAPI (blue). Scale bar for b and c indicates 50 µm.

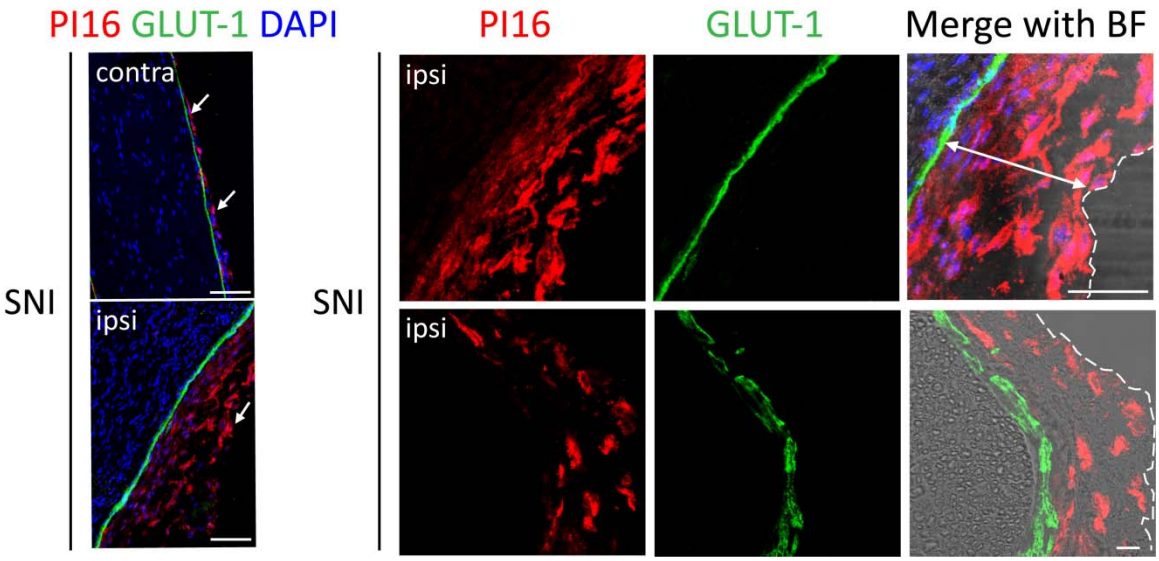

Fig. S7. Representative images for PI16 (red), GLUT-1 (green), and DAPI (blue) in sciatic nerve longitudinal sections after SNI. Note increased PI16 staining (arrow) outside GLUT-1 in ipsilateral nerve and increased thickness of epi/perineurium on the right panel (double headed arrow) in longitudinal (top) and cross section (bottom). Scale bar 100 µm (top), 25 µm (bottom).

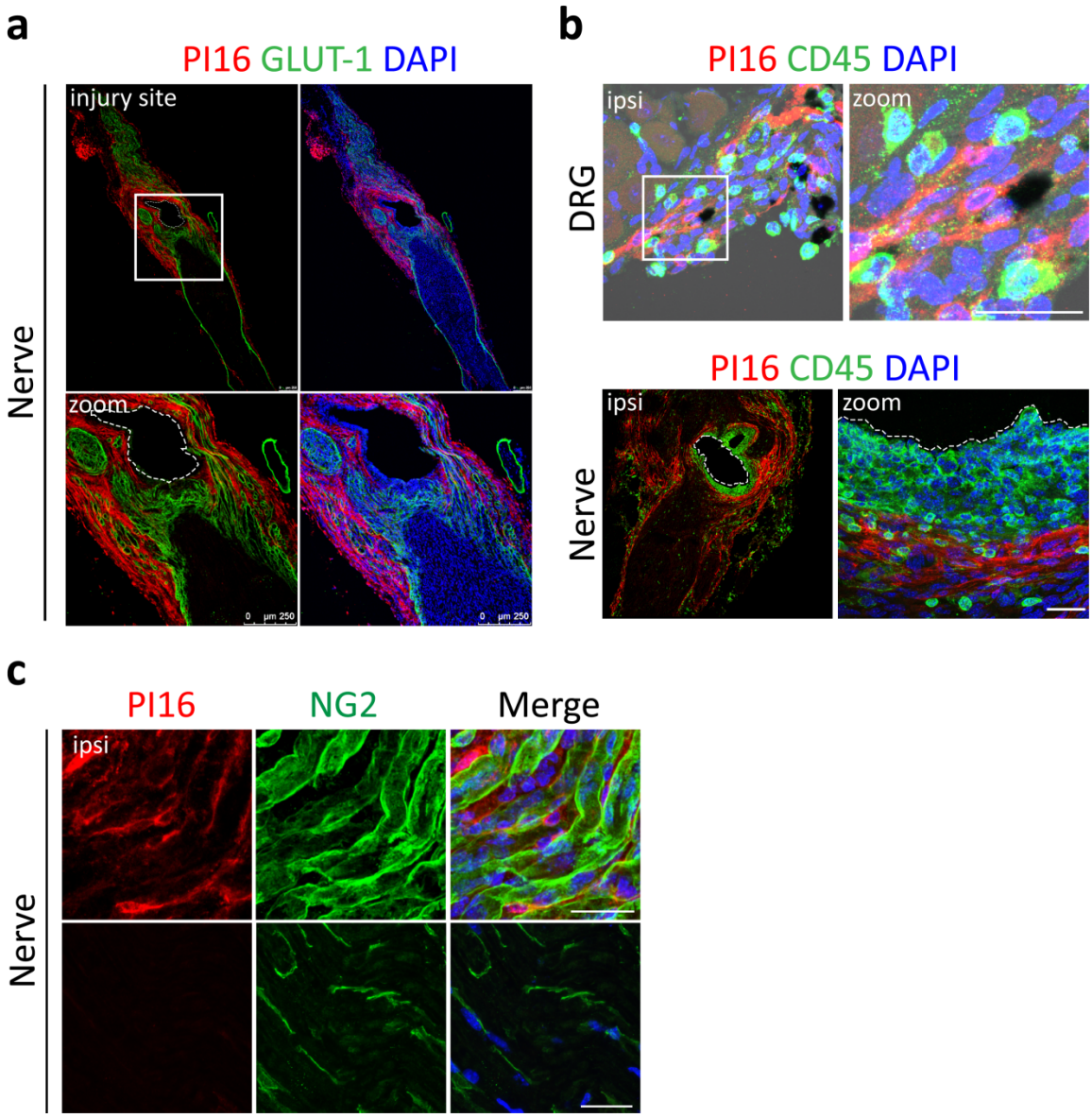

Fig. S8. PI16 is not detectable in other cells than fibroblasts. **(a)** Representative merged image showing PI16 (red), GLUT-1 (green) and DAPI (blue) immunostaining around the nerve injury site in the sciatic nerve (day 45 post SNI). White box indicates the injury site from SNI surgery and the bottom panel shows its magnified view. Scale bar indicates 250 µm. **(b)** Representative lumbar DRG and sciatic nerve section from side ipsilateral to SNI surgery showing immunostaining of PI16 (red), CD45 (green), and DAPI (blue) staining. Zoom panel shows a magnified view of the area outlined by the white square (top) and a magnified view of the nerve injury site in the sciatic nerve (bottom). Scale bar indicates 100 µm. **(c)** Representative sciatic nerve sections from the injury site showing the endoneurial cell marker NG2 (green), PI16 (red), and DAPI (blue) staining. Top panel shows an area next to the injury site and bottom panel shows endoneurial space. Scale bar indicates 100 µm.

a WT: Sham and SNI

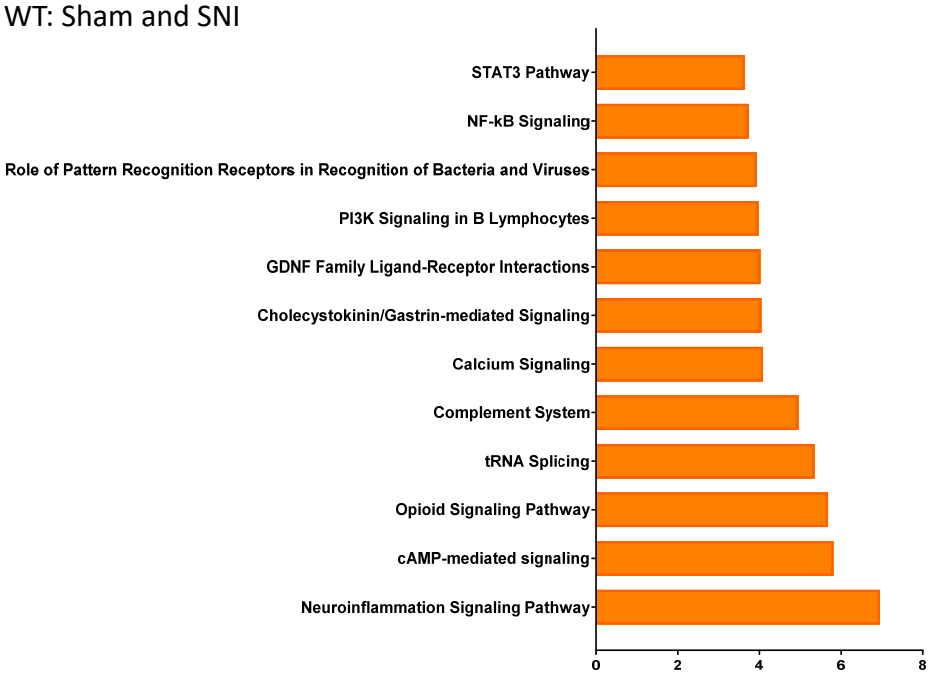

b Pi16-/- : Sham and SNI

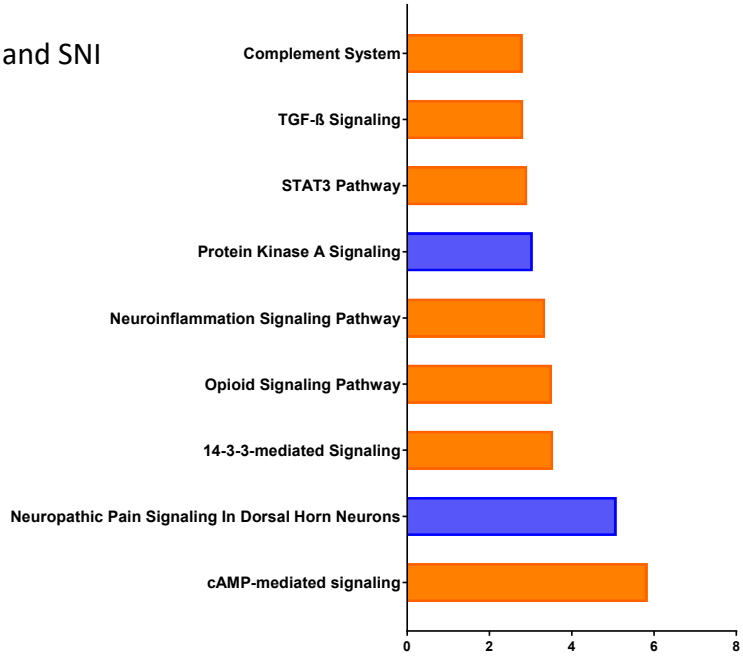

Fig. S9. Top IPA canonical pathways assigned to differentially regulated genes between **(a)** WT + Sham and WT + SNI for 956 DEG with a cutoff (−0.4 < log2 Fold Change < 0.4), p 0.05 and **(b)** Pi16 + Sham and Pi16 + SNI for 1138 DEG with a cutoff (−0.2 < log2 Fold Change < 0.2) and p 0.05. log2 Fold Change cutoff was adjusted to normalize the number of genes used for annotating canonical pathways.

WT : Sham vs SNI				
Upstream Regulator	**Expr Log Ratio**	**Activation z-score**	**p-value of overlap**	**Target molecules in dataset**
DKK3	-0.325		0.0142	ANGPT1,TAGLN
TNFSF11	0.16	3.937	5.83E-12	ADGRE1,AIF1,AQP9,ATP6V0D2,C3AR1,CCL2,Ccl8,Ccl9,CCR1,CDKN1A,CSF1R,CTSK,IFRD1,IGF1,IL13RA1,IL1RN,IL6,ITGAM,JUN,NFIL3,NFKBIZ,PLAUR,PRDM1, SDC1,SERPINE1,SPP1,SRXN1
IL24	0.237	1.204	0.0143	CASP3,GADD45A,GADD45G,PRDM1
IL7	0.341	2.42	0.000823	BTLA,CASP3,CCL2,CDKN1A,CSF1,CTSK,HAVCR2,IL1R1,IL6,Ly6a (includes others)
IL33	0.372	1.729	0.00337	ABCA1,CCR2,IL6,ITGAM,LEPR,MSR1,TIMP1
EDN1	0.376	2.985	0.0000182	ANXA1,CCL2,CYBB,EGFR,FST,IL6,ITGAM,JUN,LEPR,ODC1,PLAUR,SDC1,SERPINE1,TIMP1,TNC
CYTL1	0.399		0.0209	IGF1
CXCL12	0.424	2.354	0.000822	AIF1,CCL2,CTSK,EGFR,IL6,JUN,LOXL2,Ly6a (includes others),PPEF1,RHOC,TIMP1,TNNC1
IL1B	0.451	4.774	8.15E-17	ADAM8,AIF1,ANGPT1,ANXA1,ATF3,BAMBI,CASP3,CCKAR,CCL2,Ccl9,CCR1,CCR2,CCR5,CDKN1A,CREM,CRH,CSF1,CTSS,CX3CR1,CYBB,CYSLTR1,F13A1,FGF7,FST,GADD45A,HPGDS,Hrk,IBSP,IFI16,IFRD1,IGF1,IGFBP3,IL1R1,IL1RN,IL6,ITGAM,JUN,LAMB3,LOX,MAFA,MYLK,NFIL3,NFKBIZ,NPY,NTRK1,ODC1,PAPPA,PDE4B,PHLDA1,PTHLH,S100A10,SDC1,SERPINE1,SLC6A4,SPP1,STAR,STMN2,TIMP1,TLR7,TLR8,TREM2
Ccl6	0.466		0.0142	CTSK,CTSS
IL6	0.503	4.549	6.47E-18	ABCA1,ACVR1,ADGRE1,ANXA1,ATF3,CASP3,CCL2,CCR1,CCR2,CCR5,CD163,CD38,CD53,CD68,CDKN1A,CDKN3,CRH,CRLF1,CSF1,CTSC,CTSK, CX3CR1,CYBB,CYP1B1, EGFR,FCGR1A,GADD45A,GADD45G,GAL,GAP43,HPGD,IFI16,Ifi202b,IGF1, IGFBP3,IL1R1,IL1RN,IL6,ITGAM, ITPR1,JUN,KIF22,LGALS1,MSR1,NPY,PTPRC, REG1A,SERPINE1,SPP1,STEAP4,TH,TIMP1,TLR1,TLR7,TLR8,TNC,TNFRSF12A
SPP1	0.515	2.634	0.0000255	ANGPT1,CCL2,CD163,CDKN1A,DSP,EGFR,IGF1,IL6,LOX,SERPINE1,SNAI2,SPP1, TGFBR1,TIMP1
CCL2	0.552	1.233	0.00017	ABCA1,CCL2,CCR2,HDC,IGF1,IL6,SERPINE1,TIMP1
IL1RN	0.597	-1.637	0.000000448	ATF3,CCL2,CHAC1,CRH,CTSS,IGF1,IL6,KLF6,NTRK1,SERPINE1,SLC15A3, SLC6A4,SPP1,TIMP1
TIMP1	0.607	0	0.00477	CD38,CDKN1A,IGFBP3,PLAUR
CSF1	1.214	3.665	2.12E-08	CCL2,CCR5,CD163,CD68,CDKN1A,CSF1,CSF1R,CTSK,FCER1G, IGF1,IL6,ITGAM,JUN,MMP16,MRC1,MSR1,PTPRC,TLR1
CRH	1.57	1.498	0.00185	CRH,HPGD,IL1RN,IL6,STAR,UCN
Pi16-/-: Sham vs SNI				
Upstream Regulator	**Expr Log Ratio**	**Activation z-score**	**p-value of overlap**	**Target molecules in dataset**
IL24	0.123	-	0.0283	GADD45A,GADD45G
TIMP1	0.231	-	0.0158	CDKN1A,PLAUR
CSF1	0.883	1.981	0.024	CDKN1A,CSF1,MMP16,MRC1

Fig. S10. IPA's upstream regulator analysis was used to identify potential "cytokines" causing changes in gene expression in response to SNI in DRG between Sham and SNI group.

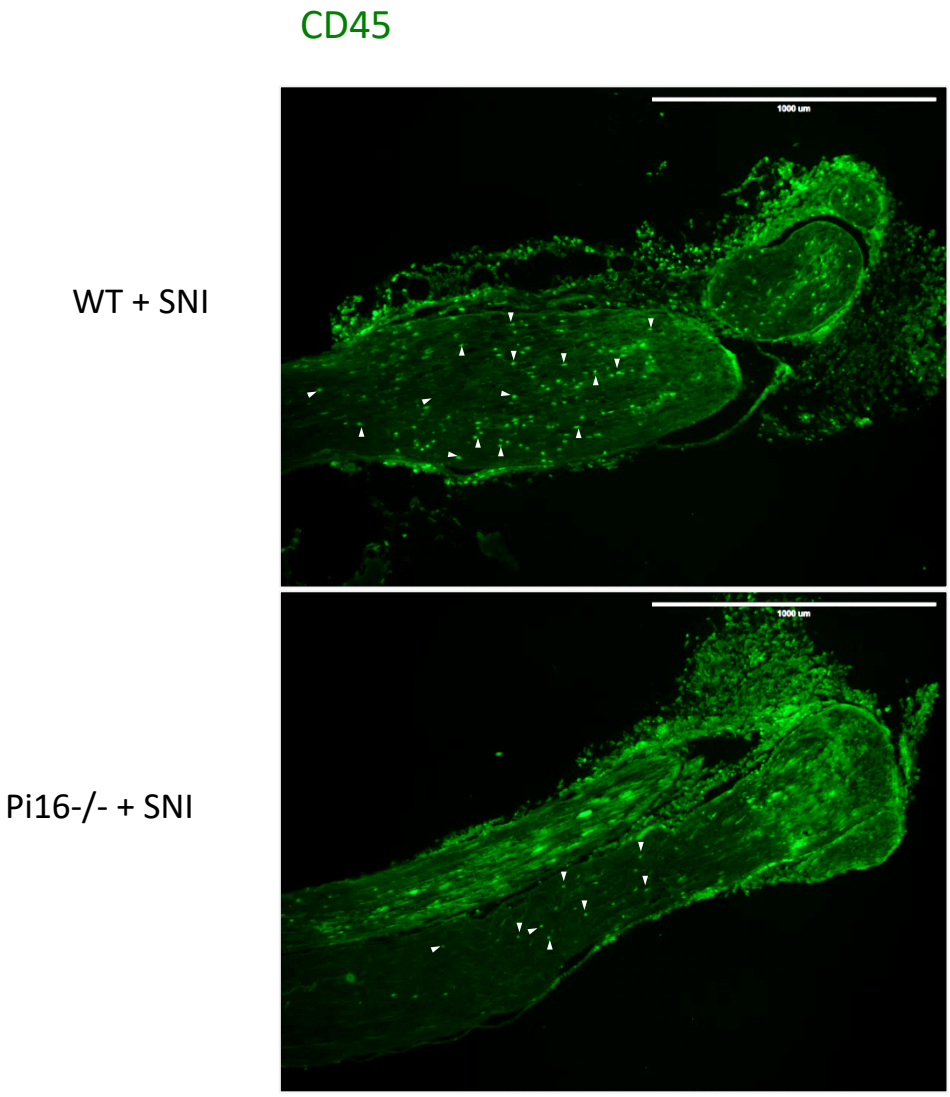

Fig. S11. Lower magnification image of sciatic nerve section with a larger field of view after SNI from the ipsilateral side (day 5) showing immunostaining of CD45 (green) in WT and Pi16-/- mice. White arrowheads indicate few of the CD45 positive cells. Note reduced number of CD45 positive cells (arrowheads) in Pi16-/- compared to WT. Scale bar indicates 1000 µm.

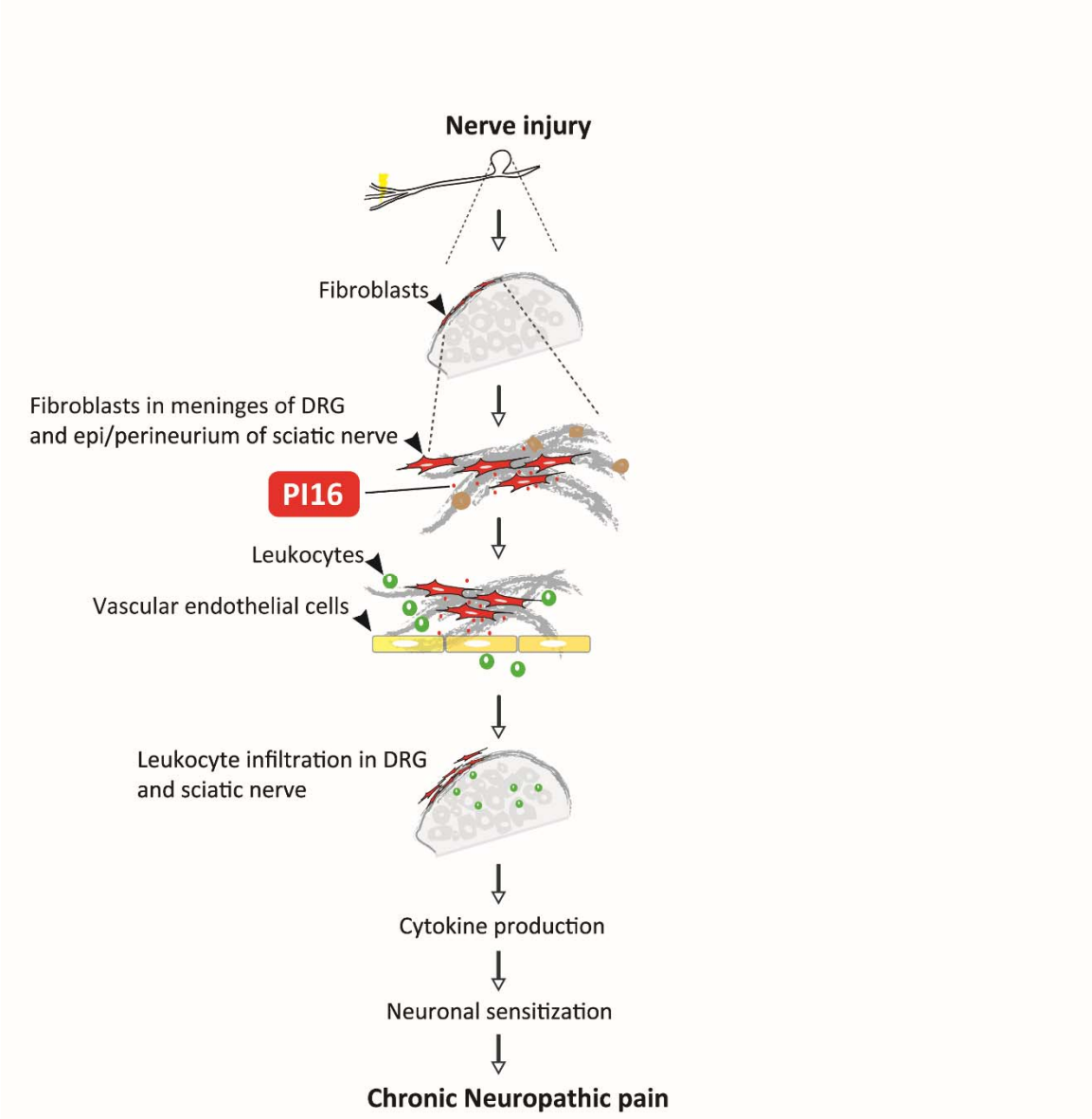

Fig. S12. Schematic summarizing the role of PI16 in chronic neuropathic pain. PI16 is expressed by meningeal fibroblasts surrounding the DRG and epi/perineurial fibroblasts around the nerve and is not detectable in neurons or glia. Spared nerve injury (SNI) induces the expansion of α-SMA positive myofibroblasts in the meninges and epi/perineurium that produce PI16. We propose that PI16 acts as a paracrine factor on vascular endothelial cells to increase the permeability of the endothelial barrier via a MLCK-dependent pathway. Our findings indicate that PI16-dependent increased endothelial permeability facilitates leukocyte infiltration into DRG and nerve thereby increasing the release of inflammatory mediators leading to increased neuronal sensitization. Our findings show that Pi16 knock out mice are protected against SNI-induced pain, increased endothelial barrier permeability and leukocyte infiltration.

References

1. Zimmermann M (1983) Ethical guidelines for investigations of experimental pain in conscious animals. *Pain* 16(2):109-110.
2. Decosterd I & Woolf CJ (2000) Spared nerve injury: an animal model of persistent peripheral neuropathic pain. *Pain* 87(2):149-158.
3. Laumet G*, et al.* (2017) Upregulation of neuronal kynurenine 3-monooxygenase mediates depression-like behavior in a mouse model of neuropathic pain. *Brain, behavior, and immunity* 66:94-102.
4. Chaplan SR, Bach FW, Pogrel JW, Chung JM, & Yaksh TL (1994) Quantitative assessment of tactile allodynia in the rat paw. *Journal of neuroscience methods* 53(1):55-63.
5. Chiu GS*, et al.* (2018) Nasal administration of mesenchymal stem cells restores cisplatin-induced cognitive impairment and brain damage in mice. *Oncotarget* 9(85):35581-35597.
6. Chiu GS*, et al.* (2017) Pifithrin-mu Prevents Cisplatin-Induced Chemobrain by Preserving Neuronal Mitochondrial Function. *Cancer research* 77(3):742-752.